

A Systems Biomedicine Approach for Chronotherapeutics Optimization: Focus on the Anticancer Drug Irinotecan

Annabelle Ballesta, Jean Clairambault, Sandrine Dulong, and Francis Levi

Abstract Most physiological functions in mammals display rhythms of period around 24 h, also called *circadian rhythms*. This temporal organization of the organism results in variations in the toxicity and efficacy of many antidrugs with respect to their circadian time of administration. Recent experimental and clinical results support the need of personalizing the chronomodulated administration pattern according to the patient genetic and circadian profile. We propose here a systems biomedicine approach for the optimization of the circadian delivery of irinotecan (CPT11), an anticancer drug approved for the treatment of colorectal cancer. First, CPT11 pharmacokinetics-pharmacodynamics (PK-PD) has been experimentally studied in Caco-2 colon cancer cell cultures. After cell synchronization, circadian rhythms with a period of 26 h 50 (SD 63 min) were observed as well as circadian variations in the protein amount of DNA-bound topoisomerase 1 in presence of CPT11, a marker of the drug PD. A mathematical model of CPT11 molecular PK-PD was then designed, fitted to experimental data and used in therapeutic optimization procedures. We adopted the therapeutics strategy of maximizing efficacy in non-synchronized cells, considered as cancer cells, under a constraint of

A. Ballesta (✉) · J. Clairambault
INRIA Paris-Rocquencourt, BANG project-team, Domaine de Voluceau, BP105, 78153 Le Chesnay Cedex, France
e-mail: annabelle.ballesta@inria.fr, jean.clairambault@inria.fr

S. Dulong
INSERM, U776 “Rythmes biologiques et cancers”, Hôpital Paul Brousse, F-94807 Villejuif, France and Université Paris-Sud, UMR-SO776, F-91405 Orsay, France
e-mail: sandrine.dulong@inserm.fr

F. Levi
INSERM, U776 “Rythmes biologiques et cancers”, Hôpital Paul Brousse, F-94807 Villejuif, France and Université Paris-Sud, UMR-SO776, F-91405 Orsay, France and Assistance Publique – Hôpitaux de Paris, Unité de Chronothérapie, Département d’oncologie médicale, Hôpital Paul Brousse, Villejuif, France
e-mail: francis.levi@inserm.fr

maximum toxicity in synchronized cells, representing healthy ones. For any dose of CPT11, optimal exposure durations varied from 3h40 to 7h10. Optimal schemes started between CT2h10 and CT2h30, a time interval corresponding to 1 h 30 to 1 h 50 before the nadir of CPT11 bioactivation rhythm in healthy cells. The second step of our approach has consisted in optimizing CPT11 administration in mice. Within the European project TEMPO, CPT11 chronotoxicity has been studied in mice and three classes have been determined with regards to CPT11 best circadian time of administration (i.e. the time which induces the minimal toxicity). We have developed a whole-body physiologically-based model of CPT11 PK-PD based on the previous *in vitro* study, which aims at identifying molecular biomarkers which could discriminate between the mouse classes and at designing optimal chronomodulated infusion scheme for each of them. Parameters of the model have been estimated for B6D2F1 male mice (chronotoxicity class 2) by fitting available data on tissular PK for two different circadian times of administration and on circadian rhythms of relevant proteins. The same parameter estimation is in progress for the two other classes, which will allow the comparison of the three parameter sets in order to identify molecular differences between the classes. Moreover, optimization algorithms will be applied to the data-calibrated model to design theoretically optimal chronomodulated scheme of administration. In a clinical perspective, this whole-body model of CPT11 PK-PD designed for mice will be adapted to humans by keeping its main structure and resizing parameter values. This will provide clinicians with a new tool towards the personalization of CPT11 administration according to the patient genetic and circadian profile.

1 Chronotherapeutics of Cancer

Most physiological functions in mammals display rhythms of period around 24 h, also called *circadian rhythms* from the latin *circa diem*, around a day. Rest-activity rhythm, core temperature, cardiac rhythm, blood pressure, or intracellular concentrations of metabolic enzymes present variations over the 24-hour span [28]. This circadian regulation allows an anticipation upon the energetic supply of the body. It contributes to the optimal control of the energy needed for the smooth functioning of the organism.

1.1 The Circadian Timing System

1.1.1 The Central Pacemaker

The circadian timing system in mammals is controlled by a central pacemaker located in the hypothalamus in the brain: the suprachiasmatic nuclei (SCN). The SCN display endogenous circadian oscillations whose period depends on the genetic background of the individual and ranges from 23 to 25 h in humans [38]. Endogeneity of those rhythms has been demonstrated by their persistence when the individual is kept under constant darkness or constant light. The self-sustained oscillating SCN

are also entrained by environmental factors such as light, socio-professional activities or food intake which exactly calibrate their period each day to 24 h [28].

The central pacemaker exerts a control on peripheral clocks through different physiological signaling. Indeed, each nucleated cell of the organism is endowed with a molecular circadian clock which is constituted of clock genes interconnected in regulation feedback loops. The structure of this gene network intrinsically generates oscillations in clock genes mRNA and protein levels which in turn induce rhythms in the expression of other genes, in particular of those involved in drug metabolism, cell cycle, DNA repair, apoptosis and angiogenesis [29].

1.1.2 Molecular Description of the Cellular Clock

To be more specific, circadian oscillations are generated by transcriptional or post-transcriptional feedback loops. Clock genes can be categorized into two groups. On one hand, the positive category is composed of transcriptional factors such as BMAL1, CLOCK, or NPAS2. On the other hand, the negative group mainly consists of Cryptochrome (Cry) and Period (Per) genes. BMAL1-CLOCK or BMAL1-NPAS2 heterodimers activate Cry and Per transcription which leads to the subsequent accumulation of CRY and PER proteins in the cytosol. Those proteins then associate into heterotypic complexes which inhibit the action of BMAL1-CLOCK/NPAS2 dimers and thus repress their own expression. This inhibition decreases CRY and PER protein amounts which goes beneath the threshold concentration allowing autorepression, and triggers a new cycle of Cry and Per transcription [29].

In parallel, positive (BMAL1, CLOCK, NPAS2) and negative (CRY, PER) transcriptional regulators respectively activate and repress the transcription of the orphan nuclear receptor *Rev - Erba*, and probably that of *Rev - Erbβ* as well. *Rev - Erba/β* proteins then strongly repress Bmal1 transcription and probably that of Clock but in a weaker manner [36]. This coupling is not mandatory to generate oscillations of the system but rather participates in the robustness of the molecular clock.

1.1.3 Experimental Assessment of the Circadian Timing System

In cell culture. Mammalian nucleated cells are endowed with a molecular circadian clock whose rhythms persist *in vitro* [4, 9, 43]. However, in the absence of an external synchronizer, the millions of cells which are contained in a single Petri dish do not oscillate neither with the same period nor with the same phase [9, 43]. Cell synchronization may be undertaken through a seric shock (exposure to a large amount of nutrient, [5]), through drug exposure [22] or temperature cycles [8]. The main effect of those synchronizers lies in the simultaneous reset of all cellular clocks which then oscillate in synchrony with a period close to 24 h. *In vitro* measurements of circadian rhythms of gene expression are then possible during several consecutive days. The time unit is then Circadian Time (CT), expressed in hours, where CT0 is the beginning of cell synchronization.

In rodents. Experimental demonstration of circadian rhythms can be undertaken in preclinical models such as the Rat or the Mouse. This involves the use of specific equipments dedicated to chronobiologic studies. They are composed of isolated shelves in which groups of animals are synchronized at different circadian stages using light control. Time is expressed in Zeitgeber Time (ZT) or in Hours After Light Onset (HALO). The typical synchronization pattern consists of an alternation of 12 hours of light and 12 hours of darkness (LD12:12). Animals can also be kept under constant darkness (DD) or constant light (LL). Animals may then be sacrificed at particular circadian stages to allow relevant biological measurements.

In humans. Minimally- or non-invasive procedures are nowadays available to provide high quality and reliable data about the patient circadian clocks and their coordination. Whenever circadian physiology is concerned, frequent sampling over several days has been advocated and used in order to provide an insight into the Circadian Timing System (CTS) of the patient. Chronobiology rhythms can be measured in patients in several ways. Rest-activity rhythms can be monitored through actimetry which has been considered as the method of choice regarding reliability, convenience and continuity in recordings [33]. Then temperature rhythms can be non-invasively assessed using different devices [33]. Moreover salivary samples can be collected in order to measure gene expression levels in the oral mucosa, those of cortisol and melatonin being considered as relevant circadian biomarkers in cancer patients [28, 33].

1.2 Current Knowledge on Chronotoxicity and Chronoefficacy of Anticancer Drugs

The circadian organization in mammals results in variations in the toxicity and efficacy of many drugs with respect to their circadian time of administration, named chronotoxicity and chronoefficacy. We focus here on the chronopharmacology of anticancer drugs.

Chronotoxicity in preclinical models. Tolerance to at least 40 anticancer agents is modified by their circadian time of administration in rats and mice [28]. Survival and maximal body weight loss after a drug administration of a potentially-lethal dose vary by a factor ranging from 2 to 10 according to the circadian time of injection. Those large differences are observed independently of the administration mode – oral, intra-peritoneal or intra-arterial – and of the number or frequency of administrations [29]. Moreover, circadian rhythms in the tolerability of anticancer drugs persist in rodents kept in constant darkness or in constant light, which demonstrates their endogeneity [39].

Optimal administration times of anticancer drugs are spread over the 24 h span and cannot be predicted by the drug pharmacological classification or main toxicity target organs [28]. The combination of chemotherapy drugs does not seem to affect their optimal administration times which remain the same observed when they are administered as single agents. In particular, this was demonstrated for the com-

bination doxorubicin-cisplatin in rats, for irinotecan-oxaliplatin and gemcitabine-cisplatin in B6D2F1 mice, and for docetaxel-doxorubicin in C3H/He mice [28]. The circadian control of the determinants of anticancer drug chronotoxicity seems to persist after the first drug exposure, at least when the latest is given at its best tolerability time [28].

Chronoefficacy in preclinical models. Circadian timing also affects the antitumor efficacy of at least 28 anticancer drugs in rodents with various kinds of malignancies [28]. Appropriately circadian-timed and dosed chemotherapy with one or several drugs at least halves tumor growth rate and/or significantly increases life span in tumor-bearing mice [28].

The circadian pattern of chronoefficacy usually coincides with that of chronotolerance. This is true for cytostatics, interferons, antiangiogenic agents, and cell cycle inhibitors, as well as for combination chemotherapy, such as irinotecan-oxaliplatin, gemcitabine-cisplatin, and docetaxel-doxorubicin, three widely used clinical regimens [28]. Experimental chronotherapeutics thus strongly supports circadian timing as a relevant method for improving anticancer treatments.

Chronotoxicity and chronoefficacy in patients with metastatic colorectal cancer. The conception of multichannel programmable delivery pumps has allowed the clinical development of cancer chronotherapeutics. Those pumps deliver a combination of anticancer drugs to non hospitalized patients, according to previously-implemented administration schemes (e.g. constant, semi-sinusoidal, linearly increasing or decreasing infusion) [28].

Over 100 phase I and II clinical trials of cancer chronotherapeutics have involved patients with advanced or metastatic cancer of almost all origins according to a PubMed search. Randomized phase III trials have compared chronotherapeutics administration schemes to their paired constant-rate infusion schedule lasting an integral multiple of 24 h and involving the same drug doses [28].

In particular, two international randomized phase III trials have compared the chronomodulated scheme ChronoFLO5 to an equivalent constant delivery in 278 patients with metastatic colorectal cancer. ChronoFLO5 combines the daily delivery of oxaliplatin over 11.5 h with peak flow rate at 4:00 p.m. and that of 5-FU-leucovorin over 11.5 h with peak flow rate at 4:00 a.m., for 5 consecutive days. The other cohort of patients received the same doses of the same three drugs, at a constant rate over the same 5-day span. In those trials, chronomodulated delivery reduced the incidence of grade 3–4 mucositis by fivefold and halved the incidence of peripheral sensory neuropathy [28].

A third randomized trial has compared the chronomodulated administration of the same three drugs over 4 days (ChronoFLO4) to a conventional constant-rate infusion over 2 days (FOLFOX2) in 564 patients with metastatic colorectal cancer. Overall survival, the main endpoint in this large international study, did not differ as a function of treatment schedule. However, the relative risk of an earlier death on ChronoFLO4 significantly increased by 38% in women and significantly decreased by 25% in men compared with conventional delivery [28]. A recent meta-analysis of these three randomized trials in 842 patients with metastatic colorectal cancer

confirms that the three-drug chronomodulated infusion achieves similar or worse efficacy compared with conventional delivery in women. In men, however, the same ChronoFLO treatment significantly increased tumor response and survival compared with conventional delivery, independently of all other prognostic factors. This result highlights the need for chronotherapeutic personalization in which chronomodulated administration schemes would be tailored according to the patient circadian and genetic profile.

2 Focus on the Anticancer Drug Irinotecan

We now focus on the anticancer drug irinotecan (CPT11) which was clinically approved for the treatment of colorectal cancer in 1994. CPT11 is part of the camptothecin family whose active principle comes from the Chinese tree *Camptotheca acuminata decne*. Other anticancer drugs are derived from the same molecule such as topotecan which is widely used for breast cancer treatment, or 9-aminocamptothecin. CPT11 administration may be responsible for severe toxicities in the bone marrow and in the intestine both in pre-clinical models and in cancer patients. The improvement of tolerability to CPT11 is thus a current clinical concern in particular in the case of digestive cancers. CPT11 toxicity and efficacy display rhythms both in mice and in cancer patients. Our approach aims at taking advantage of those circadian rhythms to reduce CPT11 toxicity and increase its efficacy.

2.1 Molecular Pharmacology of Irinotecan

Here we give molecular details about CPT11 PK-PD. CPT11 is an inhibitor of topoisomerase 1 (TOP1). The TOP1 enzyme is present in all normal nucleated cells. Its function is to relax supercoiled DNA [35]. Indeed transcription or replication mechanisms may increase the tension in DNA strands. The TOP1 enzyme wraps DNA and temporarily cuts one strand which rotates around the DNA molecule. Then TOP1 dissociates allowing the DNA strand to reconnect.

CPT11 attaches DNA/TOP1 complexes when the DNA strand is cut, thus creating CPT11/TOP1/DNA complexes whose lifetime is much longer than that of DNA/TOP1 ones. However those ternary complexes can still spontaneously dissociate. Collisions between those complexes and transcription or replication mechanisms induce irreversible single- or double-stranded DNA damage which triggers DNA repair, cell cycle arrest and may lead to cell apoptosis.

Concerning CPT11 pharmacokinetics, CPT11 is a prodrug which has to be activated into its metabolite SN38 under the activity of carboxylesterases (CES) enzymes. SN38 cytotoxic activity is a hundred to a thousand times higher than that of CPT11 [4]. SN38 is deactivated into SN38G by glucuronidation through the activity of UGT1A enzymes. The inverse reaction which consists in SN38G re-activation into SN38 occurs in several cancer cell lines and in the intestinal cells where the β -glucuronidase enzyme is expressed and catalyzes the reaction. CPT11 is converted in two other metabolites, namely APC and NPC, through the enzymatic activ-

ity of P450 3A4/3A5 cytochromes. Only NPC can be subsequently activated into SN38.

The uptake of CPT11 in the intracellular medium seems to occur in a passive manner involving a free diffusion through the cell membrane, as suggested by the absence of saturation in the uptake rate in the case of high drug concentrations [4]. Conversely, CPT11 and its metabolites are actively expelled outside of the cells by transporters of the ATP-Binding Cassette (ABC) family. Transporters involved in CPT11 efflux are mainly ABCB1 (P-gp), ABCC1 (MDR1), ABCC2 (MDR2) and ABCG2 (BCRP) [4].

2.2 Chronotoxicity and Chronoefficacy of Irinotecan

The expression of several genes involved in CPT11 PK-PD displays circadian variations in cell culture, in mice and in humans. This is the case for P450 cytochromes whose mRNA expression, protein amount and enzymatic activity vary according to the circadian time in mice and in humans [26, 34]. The activation enzymes CES1 and 2, the deactivation protein UGT1A1, the drug target TOP1 and the efflux transporters display circadian rhythms in their gene expression in cell culture and in mice [3, 4, 20, 23–25, 32, 41, 44]. Those molecular circadian rhythms induce different responses to CPT11 exposure depending on its administration time.

In mice. In B6D2F1 male mice, all toxicity criteria such as survival, body weight loss, hematological or intestinal lesions display circadian variations. CPT11 administration given as a single agent or combined with oxaliplatin is better tolerated at the end of the rest phase, at ZT11, both in GOS tumor-bearing and non-bearing mice [15, 19]. A similar chronotolerance has been observed in ICR male mice in which CPT11 intraperitoneal injection at ZT10 induce half leucopenia than the same injection performed at ZT22 [31].

Concerning CPT11 efficacy on tumor progression, CPT11 alone or in combination with oxaliplatin is more efficient when injected at ZT7 or 11 in GOS-tumor-bearing mice [19]. On the contrary, in ICR male mice bearing S-180 sarcoma, CPT11 antitumor activity is higher in mice treated at ZT10 compared to those treated at ZT22. This difference in CPT11 chronoefficacy could be explained by the fact that S-180 sarcoma is a low-growing tumor whereas GOS cancer cells proliferate much faster. Those different growth rates could be responsible for the differences in the chrono-chemosensitivity, as theoretically demonstrated in a recent study [6].

In patients with metastatic colorectal cancer. Experimental results on CPT11 chronoactivity in B6D2F1 male mice are in favor of an administration of the drug at the end of the rest phase. Thus, a chronomodulated administration scheme has been conceived for cancer patients and consists in a sinusoidal drug infusion from 2am to 8am, peaking at 5am. This delivery pattern was administered in monotherapy to patients suffering from metastatic colorectal cancer at the dose of 350 mg/m² and then in a randomized study [18, 27]. It was compared with a conventional administration of the same dose over 30 min at 10 am. Those two clinical trials involved

respectively 30 and 36 patients. They concluded to a slightly better drug tolerance in the chronomodulated cohort and to differences in CPT11 pharmacokinetics and biotransformation between the two groups of patients.

CPT11 chronotherapy has then been combined with the intravenously administered ChronoFLO4 scheme in two clinical trials. This ChronoIFLO protocol associated CPT11 with 5-FU-leucovorin and oxaliplatin in 70 colorectal cancer patients whose tumor had become resistant to conventional chemotherapies. This drug combination achieved an efficient and durable tumor control with a lower hematological toxicity than that observed when such quadritherapy was given in a constant conventional way [14, 17]. This scheme combined or not with cetuximab has been studied in several clinical trials which demonstrate an excellent antitumor activity and an acceptable toxicity, in particular concerning hematological lesions [16].

3 Optimization of Irinotecan Exposure in Cell Culture

We propose here a combined experimental and mathematical approach to optimize CPT11 circadian delivery [4]. The first step of our approach consisted in a proof of concept which involved *in vitro* experiments on human cell cultures and *in silico* mathematical modeling [4]. CPT11 molecular pharmacokinetics (PK) and pharmacodynamics (PD) were studied in human colorectal adenocarcinoma Caco-2 cells. An ODE-based mathematical model of CPT11 PK-PD was developed. It guided the design of experiments which were performed in order to estimate parameter values of the model. Optimization procedures were then applied to the data-calibrated model in order to compute theoretically optimal exposure schemes for the Caco-2 cell line.

3.1 A Mathematical Model of CPT11 PK-PD and Its Calibration to Caco-2 Cell Experimental Data

CPT11 PK-PD were experimentally studied in Caco-2 cells [4]. CPT11 accumulated in the intracellular medium where it was bioactivated into its metabolite SN38. The pre-incubation of cells with verapamil, a non-specific inhibitor of ABC transporters, increased CPT11 intracellular accumulation, thus demonstrating the involvement of those efflux pumps in CPT11 transport. After cell synchronization by a seric shock which defined the circadian time (CT) 0, circadian rhythms of period 26 h 50 (SD 63 min) were observed in the expression of the three clock genes REV-ERB α , PER2, and BMAL1; and of six metabolic genes: the drug target topoisomerase 1 (TOP1), the activation enzyme CES2, the deactivation enzyme UGT1A1, and the four ABC transporters ABCB1, ABCC1, ABCC2, ABCG2. On the contrary, TOP1 proteic level and activity remained constant. The amount of DNA-bound TOP1 in the presence of CPT11 is a PD marker of the drug and it displayed circadian rhythms as it was equal to $47 \pm 5.2\%$ of the total amount of TOP1 protein after an exposure to CPT11 at CT14, as compared to $35.5 \pm 1.8\%$ after an exposure at CT28.

Molecular pathways of CPT11 PK-PD were modeled according to biological data published in the literature and experimental results obtained in Caco-2 cells. Briefly, the intracellular uptake of CPT11, SN38 and SN38G was assumed to be passive and modeled as a free diffusion across a membrane. CPT11 and SN38 efflux were mediated respectively by *ABC_CPT* (mainly standing for the sum of activities of ABCB1, ABCC1, ABCC2) and *ABC_SN* (for ABCC1, ABCC2, ABCG2). Efflux followed Michaelis-Menten kinetics as experimentally demonstrated in the literature [4]. Diffusion from inside to outside of the cells was neglected. CPT11 was bioactivated into SN38 through CES representing the sum of all carboxylesterases activity. This pathway was also modeled by Michaelis-Menten kinetics. SN38 was expected to be deactivated into SN38G which was modeled by Michaelis-Menten kinetics in which the mathematical variable UGT stands for the sum of all UGT1As enzymatic activities.

CPT11 ability to bind to TOP1 was neglected so that SN38 was the only molecule able to stabilize DNA/TOP1 complexes into DNA/TOP1/SN38 ones (denoted by *Compl* hereafter). Those ternary complexes were able to spontaneously dissociate or could be converted into irreversible complexes (*Icompl*) after collision with transcription or replication mechanisms [4]. Parameters of this CPT11 PK-PD model were estimated from experimental data in Caco-2 cells combined with information from literature using a bootstrap approach [4].

3.2 Theoretical Optimization of CPT11 Exposure in Caco-2 Cells

Optimization procedures were then applied to the data-calibrated model in order to compute theoretically optimal exposure schemes for Caco-2 cells. Synchronized cells were considered as healthy cells and non-synchronized cells as cancer ones as the circadian organization is often disrupted in tumor tissues. The adopted therapeutics strategy consisted in maximizing DNA damage in cancer cells under the constraint that DNA damage in the healthy population remained under a tolerability threshold. We considered administration schemes in the form of a cell exposure to an initial extracellular concentration of CPT11, over 1 to 27 h, starting at a particular CT.

For all considered doses, the optimal exposure scheme consisted in administering CPT11 over 3 h 40 to 7 h 10 starting between CT2h10 and CT2h30 which corresponded to 1 h 30 to 1 h 50 before the nadir of CES protein amount [4]. The optimal schemes were not centered on the nadir of rhythm but rather extended after it, when *UGT*, *ABC_CPT* and *ABC_SN* amounts were higher and therefore protected more efficiently healthy cells. For any maximum allowed toxicity, the optimal duration did not exceed 7 h 10, highlighting the need of short exposure durations to optimally exploit the temporal difference between healthy and cancer cells. Regarding efficacy, those optimal schemes induced twice more DNA damage in cancer cells than in healthy ones. A clinical interpretation can be obtained by rescaling to 24 h those results for Caco-2 cells which displayed a period of 26 h 50. Thus, an optimal administration of CPT11 to cancer patients should result in the presence of the drug

in the blood during 3 h 30 to 6 h 30, starting 1 h 30 to 1 h 40 before the minimum value of CES activity in the patient.

4 Optimization of Irinotecan Administration in Mice

CPT11 chronotoxicity was studied in three mice strains, in both male and female animals. From this study, three classes were characterized with respect to CPT11 chronotolerance. Those recent experimental studies demonstrated the existence of three classes of mice regarding CPT11 chronotoxicity which was assessed by survival, body weight loss, intestinal and hematological toxicities [1]. Female mice of the strain B6D2F1 represented the first class and showed worst tolerability after an injection of CPT11 at ZT3 and best tolerability at ZT15. Class 2 was constituted by B6D2F1 male mice and displayed worst toxicity at ZT23 and best toxicity at ZT11. Finally, class 3 was B6CBAF1 female mice and showed worst tolerability at ZT7 and best tolerability at ZT15.

Our combined *in vivo* and *in silico* approach aimed at characterizing the three chronotoxicity classes at the molecular level and at designing optimal administration schemes for each of them. In order to address this concern, the mathematical model which was built for Caco-2 cell culture was adapted to design a whole-body physiologically-based model of CPT11 PK-PD. Parameters were estimated for class 2 (B6D2F1 male mice) by fitting both blood and tissue pharmacokinetics data together with measurements of circadian rhythms of proteins involved in CPT11 pharmacology. Similar parameter estimations are ongoing for classes 1 and 3.

4.1 A Whole-Body Physiologically-Based Model of CPT11 PK-PD

We have built a physiologically-based whole-body model of CPT11 PK-PD. It is composed of compartments which represent the simulated organs. The liver is modeled for its major part in CPT11 metabolism. Then the two main toxicity targets of the drug which are the intestine and the bone marrow are modeled, as well as the blood, and the tumor in order to take into account the drug efficacy. Finally, the Non-Eliminating Tissue (NET) compartment stands for all other tissues such as muscles or skin (Fig. 1).

CPT11 and its metabolites circulate in and out of the tumor, the bone marrow, the NET and the liver compartments through the blood circulation. concerning the intestine, it is modeled by two compartments which represent the cells of the intestinal mucosa and the intestinal lumen. A bidirectional transport is assumed between the mucosa and the lumen. Moreover, the drug and its metabolites can be transported from the intestinal cells to the liver through the hepatic portal vein. The enterohepatic circulation is modeled by a drug transport from the liver to the intestinal lumen which stands for biliary excretion [13].

Finally, renal clearance was modeled as degradation terms for CPT11, SN38 and SN38G in the blood compartment [42]. The intestinal lumen compartment

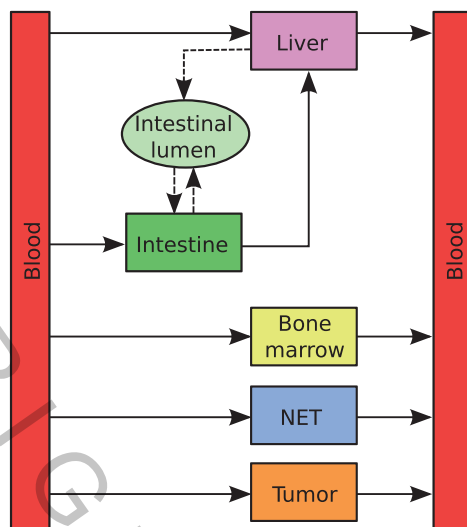


Fig. 1. Schematic view of the whole-body physiologically-based model of CPT11 PK-PD Detailed mathematical equations of the model are presented in the Appendix

presents degradation terms accounting for CPT11 and SN38 intestinal clearance, SN38G being exclusively eliminated through the kidneys [37]. Degradation speeds are assumed to be proportional to the drug concentrations. Each compartment contains an adaptation of the existing mathematical model of CPT11 tissue PK-PD as described in the following [4].

Modeling CPT11 pharmacokinetics. The uptake of CPT11 and its metabolites from the blood to the different organs is modeled as passive diffusion [4]. On the contrary, the drug efflux is assumed to be mediated by active transporters (such as ABC transporters) and is therefore modeled using Michaelis-Menten kinetics. CPT11 bioactivation into SN38 through CES activity occurs in every compartment but the NET one. SN38 glucuronidation into SN38G is assumed to be active in every compartment except in the blood and the NET compartments.

Bidirectional flux between the intestinal mucosa cells and the lumen involves active transporters in both directions [7, 40]. Intestinal cells receive the arterial blood and actively expel the drug into the portal vein, here modeled as a direct link from the intestinal compartment to the liver. The entero-hepatic circulation is represented by an active transport performed by liver cells towards the intestinal lumen through the biliary circulation. The re-activation of SN38G into SN38 under the β -glucuronidase activity only occurs in the intestinal lumen where this enzyme is produced by the bacteria of the intestinal flora. In the absence of concluding experimental data on this subject, we model this reaction by the law of mass action, in which the β -glucuronidase is in large excess compared to SN38G concentration. Differential equations of the model are presented in the Appendix.

Modeling CPT11 pharmacodynamics. The tumor, the intestine and the bone marrow being highly proliferating tissues, we have added the influence of the cell cycle on CPT11 PD to the model built in the *in vitro* study for quiescent cells. Indeed, the rate of conversion of reversible DNA/TOP1/irinotecan complexes into irreversible DNA damage depends on the cell cycle phase in which the cell stands. In the S-phase, many more replication forks run along the DNA which increases the probability of collisions with reversible complexes. This molecular mechanism may explain why CPT11 is preferentially toxic for cells in the S-phase [35]. Cyclin A ([CycA]) was used as a marker of the S-phase [30]. The speed of conversion of reversible into irreversible complexes which appears in Eqs. (3) and (4) is now assumed to be proportional to CycA concentration. Equations of CPT11 PD were adapted from the model at the tissue level as follows:

$$\frac{d[TOP1]}{dt} = k_{f_{top}} - k_{d_{top}}[TOP1] - k_{f_1}[TOP1][DNA_{free}] + k_{r_1}[DNATOP1] + k_{r_2}[Compl], \quad (1)$$

$$\frac{d[DNATOP1]}{dt} = k_{f_1}[TOP1][DNA_{free}] - k_{f_2}[DNATOP1][SN] - k_{r_1}[DNATOP1], \quad (2)$$

$$\frac{d[Compl]}{dt} = k_{f_2}[DNATOP1][SN] - k_{r_2}[Compl] - k_{Irr}[CycA][Compl], \quad (3)$$

$$\frac{d[Icompl]}{dt} = k_{Irr}[CycA][Compl]. \quad (4)$$

We assumed that CPT11 is active in mice only in the tumor, the intestine and the bone marrow as experimental results suggest [2]. Therefore CPT11 PD was modeled only in these three compartments. For the sake of simplicity, parameters k_{f_1} , k_{r_1} , k_{f_2} , k_{r_2} and k_{Irr} were assumed to be equal in all compartments and set to their values determined in the *in vitro* study [4].

Modeling pharmacological protein circadian rhythms. The protein amount of CES, UGT, CycA, TOP1 and efflux transporters of CPT11, SN38 and SN38G are assumed to display circadian rhythms in the liver, the bone marrow, the intestinal cells and lumen, and the tumor. For the sake of simplicity, we assumed that proteins of CPT11 pharmacology did not oscillate in the blood and the NET compartment. The period of oscillations was set to 24 h as mice were synchronized in LD12:12. For all proteins but TOP1, the following equation was used to model their circadian rhythms, as in the *in vitro* study [4]:

$$\frac{d[Protein]}{dt} = M + A \cos\left(\frac{2\pi}{T}(t - \phi)\right) - k_d[Protein]. \quad (5)$$

For TOP1, reaction terms presented in Eq. (1) were added to Eq. (5).

Initial conditions. At the initial instant, CPT11 was administered to the mice by intravenous injection. All variables representing the drug or its metabolites concentrations were set to zero except CPT11 blood concentration CPT_{blood} . Variables of the drug PD were set to their steady state values [4]. Concerning pharmacological protein concentrations, their numerical values were firstly computed over 24 h in the absence of CPT11, with an initial condition set to 1. Then, the computed values were used as initial condition for considered ZTs.

4.2 Model Calibration for B6D2F1 Male Mice

A set of parameters was estimated for B6D2F1 male mice (class 2 of the three chronotoxicity classes). Mainly two kinds of experimental data were used for parameter estimation. On one hand, protein amounts were assessed over the 24 h span for *ces1*, *ugt1a1* and *top1* in the liver; *ces1*, *ugt1a1*, *top1* and *cyclin A2* in the colon; and *abcc2* in the ileum. On the other hand, blood and tissue concentrations of CPT11 and SN38 were measured after a CPT11 injection at the worst and best circadian time regarding tolerability. Parameter estimation consisted in a least-squares approach in which the minimization task was performed by the CMAES algorithm [21]. Initial search values were set to parameter values determined in the *in vitro* study on Caco-2 cells.

Estimation of parameters of pharmacological protein circadian expression. Circadian variations of proteins of interest were measured in mice synchronized in LD12:12. Animals were sacrificed at indicated circadian times and their organs were collected. Protein quantities were then assessed by immunohistochemistry. Protein expression was determined for *ces1*, *ugt1a1* and *top1* in the liver; *ces1*, *ugt1a1*, *top1* and *cyclin A2* in the colon; and *abcc2* in the ileum [1, 2, 32]. Time series were normalized by dividing all values by the mean (Fig. 2).

Eq. (5) was used to simulate protein amounts. M and kd of Eq. (5) were set to 1, so that the mean value of simulated quantities is equal to 1. Amplitude A is searched between 0 and 1 and phase ϕ between 0 and 24 h. For each of the above-mentioned proteins in each compartment, Eq. (5) was calibrated to normalized experimental data. Estimated values of A and ϕ are shown in Table 1. In the whole-body mathematical model, parameter values of Table 1 were used to set amplitudes and phases of corresponding proteins in mentioned compartments. Circadian variations of *TOP1* and *CycA* in the bone marrow were assumed to be the same as those in the colon as no experimental data was available. Furthermore, they were set to constant values in the tumor compartment.

In the absence of relevant biological data on the circadian rhythms of ABC transporter activity at the tissue level, we assumed simplification hypotheses which may be improved in a future version of the model. Thus, efflux transporters from the intestine cells towards the intestinal lumen and the liver were assumed to display the same circadian variations. Moreover, we set circadian rhythms for the transport from the intestine cells to the lumen, but not for the opposite direction which was considered as constant. Finally, transporters in liver cells were assumed to display

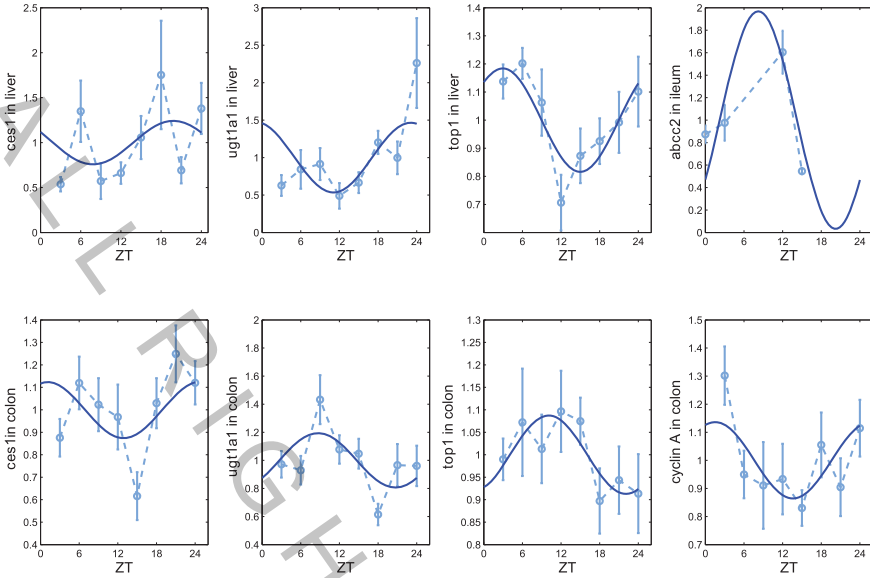


Fig. 2. Circadian variations of proteins involved in CPT11 pharmacology in B6D2F1 male mice synchronized in LD12:12. Data points represent the average of 10 to 15 animals (\pm SEM). The solid curves show Eq. (5) which was calibrated to experimental data by a least square approach. Estimated parameter values are shown in Table 1.

Table 1. Estimated parameter values for circadian rhythms of proteins of CPT11 pharmacology. Values were computed by comparing Eq. (5) to experimental data using a least square approach. a.u. = arbitrary units

<i>Proteins</i>	<i>Amplitude A (a.u.h⁻¹)</i>	<i>Phase ϕ (h)</i>
LIVER		
ces1	0.25	18.85
top1	0.19	2.0
ugt1a1	0.48	22.09
COLON		
ces1	0.13	23.93
top1	0.09	9.1
ugt1a1	0.2	7.7
cyclin A2	0.14	0.63
ILEUM		
abcc2	1	7.25

Table 2. Parameter values for circadian rhythms of proteins of CPT11 pharmacology. Parameters were estimated using experimental results on blood and tissular pharmacokinetics of CPT11 and SN38

<i>Genes</i>	<i>A (a.u.)</i>	ϕ (h)
<i>ABC_CPT_{liver_blood}</i>	0.9	6.5
<i>ABC_SN_{liver_blood}</i>	0.75	16
<i>ABC_CPT_{int_lum}</i>	0.2	7.8
<i>ABC_SN_{int_lum}</i>	0.6	22.5
<i>ABC_CPT_{marrowle_blood}</i>	0.4	9.78
<i>ABC_SN_{marrowle_blood}</i>	0	-
<i>UGT_{marrow}</i>	0.5	7
<i>ABC_CPT_{tumor_blood}</i>	0.9	6.2
<i>ABC_SN_{tumor_blood}</i>	0	—
<i>CES_{tumor}</i>	0	—
<i>UGT_{tumor}</i>	0	—

the same rhythms whether they efflux the drug into the intestine or into the blood. Amplitudes and phases of all efflux transporters were inferred from ChronoPK data (Table 2). During parameter estimation, initial values of protein quantities were set as follows. Parameter search was run a first time in order to get optimal values of A and ϕ for each gene. then the value at $t = 24$ h of the best-fit curve was used as an initial condition during the second run of parameter estimation which provided us with the final optimal parameter values. Of note, the influence of initial condition on parameters A and ϕ slightly change them by approximately 1% of their value.

4.2.1 Estimation of PK-PD Parameters

Kinetic parameters of the whole-body model were evaluated using data on CPT11 and SN38 concentrations in the blood and the tissues of interest, after a CPT11 injection at best and worst circadian time regarding toxicity. Experimental study of CPT11 PK in chronotoxicity class 2 (B6D2F1 male mice) involved animals synchronized in LD12:12 which underwent an intravenous injection of CPT11 at the dose of 50 mg/kg, at ZT11 and ZT23, which are respectively the best and worst times for tolerability. Mice were sacrificed 30 min, 1, 2, 6 and 18 h after the drug injection and tissues of interest were collected. CPT11 and SN38 concentrations were determined in the blood, the liver, the intestine cells, the bone marrow and the tumor by High Performance Liquid Chromatography (HPLC, [1]).

In the mathematical model, initial drug concentrations were all equal to zero except that of CPT11 in the blood compartment which was set to 860 μM . This cor-

responds to a dose of 50 mg/kg for a B6D2F1 male mouse whose average weight was estimated at $w = 26$ g and blood volume at $V_{blood} = 1.7\text{mL}$ [1, 12]. Values of other organ volumes were inferred from literature: $V_{liver} = 1.3\text{mL}$, $V_{intestine} = 1.5\text{mL}$, $V_{marrow} = 1.8\text{mL}$, $V_{NET} = 16\text{mL}$, $V_{tumor} = 1\text{mL}$ [12].

For the sake of simplicity, uptake and efflux parameters for SN38G were assumed to be equal to those for SN38, except for those of the entero-hepatic circulation. Moreover we have set all Km parameters of Michaelis-Menten kinetics to the values determined in the *in vitro* study. Thus, Km for CPT11 bioactivation was set to $K_{CES} = 146\mu\text{M}$, that for SN38 deactivation to $K_{UGT} = 2.85\mu\text{M}$, that for CPT11 transport to $K_{CPT} = 47.8\mu\text{M}$ and that for SN38 and SN38G transport to $K_{SN} = 1.6\mu\text{M}$. Parameters of CPT11 PD were set to their values determined in the *in vitro* study [4].

Remaining parameters were estimated by confronting the model to biological data on CPT11 and SN38 concentrations in the blood, the liver, the intestinal cells, the bone marrow and the tumor, after an injection of CPT11 at ZT11 or at ZT23. For each compartment, experimentally-observed CPT11 concentration was compared with the corresponding mathematical variable, namely CPT_{organ} . Measured concentrations of SN38 were compared to the sum of $SN_{organ} + COMPL + Icompl$ as the experimental method assessed the totality of intracellular SN38, including molecules linked to DNA. Estimated parameter values are showed in the Appendix. The data-calibrated whole-body model mimics the main features observed in the biological data of chronotoxicity class 2 (Figs. 3 and 4).

Interpretation of estimated parameter values. Concerning CPT11 uptake, the drug seemed to enter preferentially in the liver and in the NET compartments (see parameter values in the appendix). A high SN38 uptake rate was estimated in the target organs (intestine cells, bone marrow) and in the tumor which may explain the observed toxicities and efficacy in those compartments [1].

CPT11 bioactivation into SN38 was mainly present in the liver compartment and weakly active in the blood and in the bone marrow. CES activity was estimated to values close to zero in the intestinal cells where SN38 experimentally appeared 2 h after CPT11 injection, despite the presence of CPT11 in the same organ only 30 min after its injection. CPT11 metabolism in the tumor was also estimated to quasi-zero.

SN38 glucuronidation appeared to be high in the bone marrow, and less active in the liver, the intestine and the tumor.

5 Discussion and Perspectives

Current clinical knowledge supports a personalization of chronomodulated delivery regimens according to the patient circadian and genetic profile. We propose here a combined biological and mathematical approach for the optimization of CPT11 circadian delivery. CPT11 chronomodulated exposure was optimized in cultured Caco-2 cells. This *in vitro* study provided the basis for the design of a whole-body

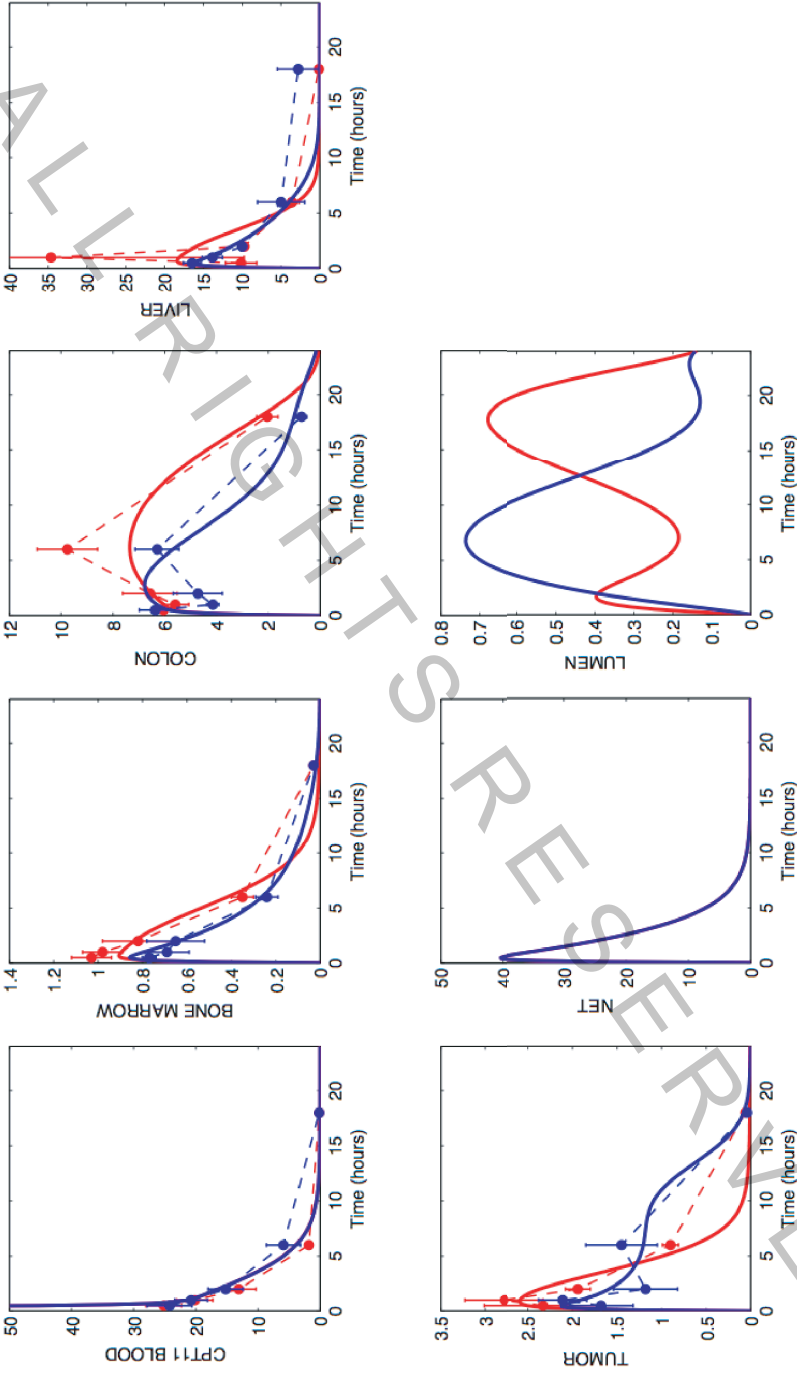


Fig. 3. Blood and tissue CPT11 PK in class 2, after injection at best (ZT11, blue) and worst (ZT23, red) time regarding toxicity. Data points stand for the mean value (\pm SEM) of 10 to 15 mice. Solid curves represent the best-fit simulations of the whole-body model

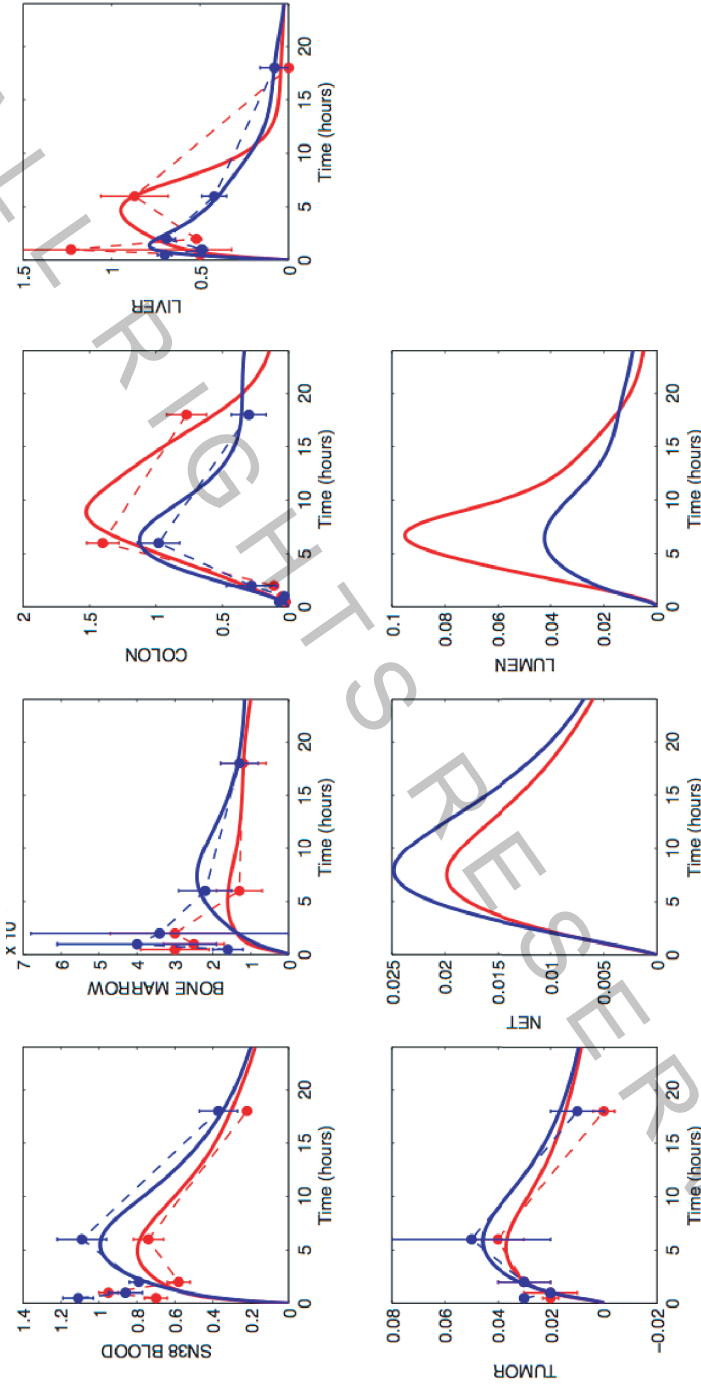


Fig. 4. Blood and tissue SN38 PK in class 2, after injection at best (ZT11, blue) and worst (ZT23, red) time regarding toxicity. Data points stand for the mean value ($\pm SEM$) of 10 to 15 mice. Solid curves represent the best-fit simulations of the whole-body model

physiologically-based model of CPT11 PK-PD which aims at optimizing CPT11 administration in three chronotoxicity classes in mice.

The whole-body model was calibrated to experimental data obtained for class 2 (B6D2F1 male mice). It provided simulations which were consistent with biological results. It also suggested molecular explanations for CPT11 and SN38 chronoPK which could lead to predictive biomarkers of CPT11 chronotoxicity in this chronotoxicity class.

The next step will consist in applying optimization procedures to the calibrated whole-body model in order to design theoretically optimal administration schemes for this class. The same study is in progress for classes 1 (B6D2F1 female mice) and 3 (B6CBAF1 female mice). Once the three parameter sets have been estimated, their comparison may allow the molecular characterization of the three classes by highlighting differences in protein activities.

The data-calibrated whole body model simulated the main features observed in the biological data of class 2 (Figs. 3 and 4). However, the rebound in CPT11 intestine concentration which occurred 2 h after the injection at the best time of tolerability (ZT11) was not captured by the model. SN38 blood concentrations were underestimated in the simulations during the first hours after CPT11 injection, which probably induced the under-estimation in SN38 bone marrow concentration during the same period of time.

In the tumor compartment, parameter estimation led us to conclude to an absence of circadian rhythms of all protein activities, except in CPT11 efflux. This suggests an absence of circadian organization in the cancer tissues; the rhythm found in CPT11 efflux may be interpreted as a circadian variation of the permeability of healthy cells in the tumor environment. Indeed, drug uptake from the blood to the tumor was assumed to be constant in the current mathematical model. This should be modified in a future version of the model.

Experimental data are available on intestinal and hematological chronotoxicities, together with chronoefficacy results on tumor growth for the three mouse classes. They are currently being integrated into the parameter estimation and will especially allow a more precise evaluation of circadian rhythms of TOP1 and CycA in the intestine, the bone marrow and the tumor. Parameters of CPT11 PD will also be adjusted.

In vitro experiments on human blood sample have demonstrated that CPT11 and SN38 associate with blood components such as plasmatic proteins, platelets or red blood cells [10, 11]. 60 to 66% of CPT11 molecules were linked to blood components when investigating CPT11 concentrations from 100 to 4000 ng/mL, whereas 94 to 96% of SN38 was linked with blood components for investigated SN38 concentrations from 50 to 200 ng/mL. These associations may interfere with the drug PK-PD and will therefore be integrated into a future version of the model. Moreover, CPT11 metabolism through P450 cytochromes should also be added to the model as it may also display circadian rhythms [26].

In a clinical perspective, this whole-body model of CPT11 PK-PD designed for mice will be adapted to humans by keeping its main structure and resizing parameter values. This will provide clinicians with a new tool towards the personalization of CPT11 administration according to the patient genetic and circadian profile.

Appendix

Equations of the Whole-Body Model of CPT11 PK-PD

Equations of the whole body physiologically-based model of CPT11 PK-PD. *int* stands for intestine, *lum* for intestinal lumen, *marrow* for bone marrow.

Liver:

$$\frac{d[CPT_{liver}]}{dt} = C_{blood_liver} - C_{liver_blood} + C_{int_liver} - \frac{V_{lum}}{V_{liver}} C_{liver_bile} - C_{CES_liver}; \quad (6)$$

$$\frac{d[SN_{liver}]}{dt} = S_{blood_liver} - S_{liver_blood} + S_{int_liver} - \frac{V_{lum}}{V_{liver}} S_{liver_bile} + C_{CES_liver} - S_{UGT_liver} + S_{RC_liver} - S_{C_liver}; \quad (7)$$

$$\frac{d[SNG_{liver}]}{dt} = G_{blood_liver} - G_{liver_blood} + G_{int_liver} - \frac{V_{lum}}{V_{liver}} G_{liver_bile} + S_{UGT_liver}. \quad (8)$$

Intestine:

$$\frac{d[CPT_{int}]}{dt} = C_{blood_int} - \frac{V_{liver}}{V_{int}} C_{int_liver} + C_{lum_int} - C_{int_lum} - C_{CES_int}; \quad (9)$$

$$\frac{d[SN_{int}]}{dt} = S_{blood_int} - \frac{V_{liver}}{V_{int}} S_{int_liver} + S_{lum_int} - S_{int_lum} + C_{CES_int} - S_{UGT_int} + S_{RC_int} - S_{C_int}; \quad (10)$$

$$\frac{d[SNG_{int}]}{dt} = G_{blood_int} - \frac{V_{liver}}{V_{int}} G_{int_liver} + G_{lum_int} - G_{int_lum} + S_{UGT_liver}. \quad (11)$$

Intestinal lumen:

$$\frac{d[CPT_{lum}]}{dt} = \frac{V_{int}}{V_{lum}} (C_{int_lum} - C_{lum_int}) + C_{liver_bile} - C_{clear_int}; \quad (12)$$

$$\frac{d[SN_{lum}]}{dt} = \frac{V_{int}}{V_{lum}} (S_{int_lum} - S_{lum_int}) + S_{liver_bile} - S_{clear_int} + G_{beta}; \quad (13)$$

$$\frac{d[SNG_{lum}]}{dt} = \frac{V_{int}}{V_{lum}} (G_{int_lum} - G_{lum_int}) + G_{liver_bile} - G_{beta}. \quad (14)$$

Bone marrow:

$$\frac{d[CPT_{marrow}]}{dt} = C_{blood_marrow} - C_{marrow_blood} - C_{CES_marrow}; \quad (15)$$

$$\begin{aligned} \frac{d[SN_{marrow}]}{dt} = & S_{blood_marrow} - S_{marrow_blood} + C_{CES_marrow} \\ & - S_{UGT_marrow} + S_{RC_marrow} - S_{C_marrow}; \end{aligned} \quad (16)$$

$$\frac{d[SNG_{marrow}]}{dt} = G_{blood_marrow} - G_{marrow_blood} + S_{UGT_liver}. \quad (17)$$

Net:

$$\frac{d[CPT_{NET}]}{dt} = C_{blood_NET} - C_{NET_blood}; \quad (18)$$

$$\frac{d[SN_{NET}]}{dt} = S_{blood_NET} - S_{NET_blood} + S_{RC_NET} - S_{C_NET}; \quad (19)$$

$$\frac{d[SNG_{NET}]}{dt} = G_{blood_NET} - G_{NET_blood}. \quad (20)$$

Tumor:

$$\frac{d[CPT_{tumor}]}{dt} = C_{blood_tumor} - C_{tumor_blood} - C_{CES_tumor}; \quad (21)$$

$$\begin{aligned} \frac{d[SN_{tumor}]}{dt} = & S_{blood_tumor} - S_{tumor_blood} + C_{CES_tumor} - S_{UGT_tumor} \\ & + S_{RC_tumor} - S_{C_tumor}; \end{aligned} \quad (22)$$

$$\frac{d[SNG_{tumor}]}{dt} = G_{blood_tumor} - G_{tumor_blood} + S_{UGT_tumor}. \quad (23)$$

Blood:

$$\begin{aligned} \frac{d[CPT_{blood}]}{dt} = & \frac{V_{liver}}{V_{blood}} (C_{liver_blood} - C_{blood_liver}) - \frac{V_{int}}{V_{blood}} C_{blood_int} \\ & + \frac{V_{marrow}}{V_{blood}} (C_{marrow_blood} - C_{blood_marrow}) \\ & + \frac{V_{NET}}{V_{blood}} (C_{NET_blood} - C_{blood_NET}) \\ & + \frac{V_{tumor}}{V_{blood}} (C_{tumor_blood} - C_{blood_tumor}) \\ & - C_{CES_blood} - C_{clear_ren}; \end{aligned} \quad (24)$$

$$\begin{aligned}
\frac{d[SN_{blood}]}{dt} = & \frac{V_{liver}}{V_{blood}}(S_{liver_blood} - S_{blood_liver}) - \frac{V_{int}}{V_{blood}}S_{blood_int} \\
& + \frac{V_{marrow}}{V_{blood}}(S_{marrow_blood} - S_{blood_marrow}) \\
& + \frac{V_{NET}}{V_{blood}}(S_{NET_blood} - S_{blood_NET}) \\
& + \frac{V_{tumor}}{V_{blood}}(S_{tumor_blood} - S_{blood_tumor}) + C_{CES_blood} \\
& - S_{clear_ren}; \tag{25}
\end{aligned}$$

$$\begin{aligned}
\frac{d[SNG_{blood}]}{dt} = & \frac{V_{liver}}{V_{blood}}(G_{liver_blood} - G_{blood_liver}) - \frac{V_{int}}{V_{blood}}G_{blood_int} \\
& + \frac{V_{marrow}}{V_{blood}}(G_{marrow_blood} - G_{blood_marrow}) \\
& + \frac{V_{NET}}{V_{blood}}(G_{NET_blood} - G_{blood_NET}) \\
& + \frac{V_{tumor}}{V_{blood}}(G_{tumor_blood} - G_{blood_tumor}) - G_{clear_ren}. \tag{26}
\end{aligned}$$

Fluxes of Equations of the Whole Body Physiologically-Based Model of CPT11 PK-PD (Organ Designates Liver, Intestine, Bone Marrow, Tumor or NET)

Cellular uptake:

$$C_{blood_organ} = k_{upCPT_organ}[CPT_{blood}]; \tag{27}$$

$$S_{blood_organ} = k_{upSN_organ}[SN_{blood}]; \tag{28}$$

$$G_{blood_organ} = k_{upSN_organ}[SNG_{blood}]. \tag{29}$$

Active transport:

$$C_{organ_blood} = \frac{V_{effCPT}[ABC_CPT][CPT_{organ}]}{K_{effCPT} + [CPT_{organ}]}; \tag{30}$$

$$S_{organ_blood} = \frac{V_{effSN}[ABC_SN][SN_{organ}]}{K_{effSN} + [SN_{organ}]}; \tag{31}$$

$$G_{organ_blood} = \frac{V_{effSN}[ABC_SN][SNG_{organ}]}{K_{effSN} + [SNG_{organ}]}; \tag{32}$$

$$C_{int_lum} = \frac{V_{int_lumCPT}[ABC_CPT_int_lum][CPT_{int}]}{K_{int_lumCPT} + [CPT_{int}]}; \quad (33)$$

$$S_{int_lum} = \frac{V_{int_lumSN}[ABC_SN_int_lum][SN_{int}]}{K_{int_lumSN} + [SN_{int}]}; \quad (34)$$

$$G_{int_lum} = \frac{V_{int_lumSN}[ABC_SN_int_lum][SNG_{int}]}{K_{int_lumSN} + [SNG_{int}]}; \quad (35)$$

$$C_{lum_int} = \frac{V_{lum_intCPT}[ABC_CPT_lum_int][CPT_{lum}]}{K_{lum_intCPT} + [CPT_{lum}]}; \quad (36)$$

$$S_{lum_int} = \frac{V_{lum_intSN}[ABC_SN_lum_int][SN_{lum}]}{K_{lum_intSN} + [SN_{lum}]}; \quad (37)$$

$$G_{lum_int} = \frac{V_{lum_intSN}[ABC_SN_lum_int][SNG_{lum}]}{K_{lum_intSN} + [SNG_{lum}]}; \quad (38)$$

PT11 bioactivation into SN38:

$$C_{CES_organ} = \frac{V_{CES_organ}[CES][CPT_{organ}]}{K_{CES} + [CPT_{organ}]}; \quad (39)$$

SN38 glucuronidation into SN38G

$$S_{UGT_organ} = \frac{V_{UGT_organ}[UGT][SN_{organ}]}{K_{UGT} + [SN_{organ}]}; \quad (40)$$

Entero-hepatic circulation

$$C_{liver_int} = \frac{V_{bileCPT}[ABC_CPT_bile][CPT_{liver}]}{K_{bileCPT} + [CPT_{liver}]}; \quad (41)$$

$$S_{liver_int} = \frac{V_{bileSN}[ABC_SN_bile][SN_{organ}]}{K_{bileSN} + [SN_{liver}]}; \quad (42)$$

$$G_{liver_int} = \frac{V_{bileSN}[ABC_SN_bile][SNG_{organ}]}{K_{bileSN} + [SNG_{liver}]}; \quad (43)$$

β -glucuronidase:

$$G_{beta} = V_{beta}[SNG_{lum}]K_{beta} + [SNG_{lum}]; \quad (44)$$

Renal and intestinal clearance:

$$C_{clear_ren} = k_{renCPT}[CPT_{blood}]; \quad (45)$$

$$S_{clear_ren} = k_{renSN}[SN_{blood}]; \quad (46)$$

$$G_{clear_ren} = k_{renSNG}[SNG_{blood}]; \quad (47)$$

$$C_{clear_int} = k_{intCPT}[CPT_{lum}]; \quad (48)$$

$$S_{clear_int} = k_{intSN}[SN_{lum}]. \quad (49)$$

PD:

$$S_{C_organ} = k_{f2}[DNATOP1_{organ}][SN_{organ}]; \quad (50)$$

$$S_{RC_organ} = k_{r2}[Compl_{organ}]. \quad (51)$$

Parameter Values

Parameter values of the whole-body model of CPT11 PK-PD, for class2 (B6D2F1 male mice). Parameters were estimated by a least square approach using the CMAES algorithm for minimization tasks.

Cellular uptake (h^{-1})

$$k_{upCPT_liver} = 0.16, k_{upSN_liver} = 0.05;$$

$$k_{upCPT_int} = 0.048, k_{upSN_int} = 0.48;$$

$$k_{upCPT_marrow} = 0.008, k_{upSN_marrow} = 0.9;$$

$$k_{upCPT_NET} = 0.4, k_{upSN_NET} = 0.23;$$

$$k_{upCPT_tumor} = 0.021, k_{upSN_tumor} = 0.45.$$

Active transport (μMh^{-1})

$$V_{liver_bloodCPT} = 14, V_{liver_bloodSN} = 28;$$

$$V_{marrow_bloodCPT} = 17, V_{marrow_bloodSN} = 6000;$$

$$V_{NET_bloodCPT} = 60, V_{NET_bloodSN} = 8;$$

$$V_{tumor_bloodCPT} = 17, V_{tumor_bloodSN} = 30;$$

$$V_{int_lumCPT} = 60, V_{int_lumSN} = 0.002, V_{int_lumSNG} = 15;$$

$$V_{lum_intCPT} = 0.001, V_{lum_intSN} = 15, V_{lum_intSNG} = 0.001.$$

CPT11 bioactivation into SN38 (μMh^{-1})

$$V_{CES_blood} = 10.5, \quad V_{CES_liver} = 35, \quad V_{CES_int} = 0.02,$$

$$V_{CES_marrow} = 10, \quad V_{CES_tumor} = 0.001.$$

SN38 glucuronidation into SN38G (μMh^{-1})

$$V_{UGT_liver} = 80, \quad V_{UGT_int} = 20, \quad V_{UGT_marrow} = 5000,$$

$$V_{UGT_tumor} = 300.$$

Entero-hepatic circulation (μMh^{-1})

$$V_{bileCPT} = 0.01, \quad V_{bileSN} = 0.4\mu M.$$

 β -glucuronidase

$$V_{beta} = 20\mu Mh^{-1}, \quad K_{beta} = 10\mu M.$$

Renal and intestinal clearance (h^{-1})

$$k_{renCPT} = 4.2, \quad k_{renSN} = 0.3, \quad k_{renSNG} = 0.5,$$

$$k_{intCPT} = 1, \quad k_{intSN} = 8.$$

References

1. Ahowesso, C.: Approche expérimentale de la personnalisation de la chronothérapeutique par irinotecan. Thèse Université Paris-Sud 11 (2011)
2. Ahowesso, C., Piccolo, E., Li, X.M., Dulong, S., Hossard, V., La Sorda, R., Filipski, E., Tinari, N., Delaunay, F., Iacobelli, S., Levi, F.: Relations between strain and gender dependencies of irinotecan toxicity and UGT1A1, CES2 and TOP1 expressions in mice. *Toxicol. Lett.* **192**, 395–401 (2010)
3. Ando, H., Yanagihara, H., Sugimoto, K., Hayashi, Y., Tsuruoka, S., Takamura, T., Kaneko, S., Fujimura, A.: Daily rhythms of P-glycoprotein expression in mice. *Chronobiol. Int.* **22**, 655–665 (2005)
4. Ballesta, A., Dulong, S., Abbara, C., Cohen, B., Okyar, A., Clairambault, J., Levi, F.: A combined experimental and mathematical approach for molecular-based optimization of irinotecan circadian delivery. *PLoS Comput. Biol.* **7**, e1002143 (2011)
5. Balsalobre, A., Damiola, F., Schibler, U.: A serum shock induces circadian gene expression in mammalian tissue culture cells. *Cell* **93**, 929–937 (1998)
6. Bernard, S., Cajavec-Bernard, B., Levi, F., Herzel, H.: Tumour growth rate determines the timing of optimal chronomodulated treatment schedules. *PLoS Comput. Biol.* **3**, e1000712 (2010)
7. Brand, W., Schutte, M.E., Williamson, G., van Zanden, J.J., Cnubben, N.H., Groten, J.P., van Bladeren, P.J., Rietjens, I.M.: Flavonoid-mediated inhibition of intestinal ABC transporters may affect the oral bioavailability of drugs, food-borne toxic compounds and bioactive ingredients. *Biomed. Pharmacother.* **60**, 508–519 (2006)
8. Brown, S.A., Zumbern, G., Fleury-Olela, F., Preitner, N., Schibler, U.: Rhythms of mammalian body temperature can sustain peripheral circadian clocks. *Curr. Biol.* **12**, 1574–1583 (2002)
9. Carr, A.J., Whitmore, D.: Imaging of single light-responsive clock cells reveals fluctuating free-running periods. *Nat. Cell. Biol.* **7**, 319–321 (2005)

10. Chabot, G.G., Robert, J., Lokiec, F., Canal, P.: Irinotecan pharmacokinetics. *Bull. Cancer. Spec No:*11–20 (1998)
11. Combes, O., Barré, J., Duché, J.C., Vernillet, L., Archimbaud, Y., Marietta, M.P., Tillement, J.P., Urien, S.: In vitro binding and partitioning of irinotecan (cpt-11) and its metabolite, sn-38, in human blood. *Invest. New Drugs*. **18**, 1–5 (2000)
12. Davies, B., Morris, T.: Physiological parameters in laboratory animals and humans. *Pharm. Res.* **10**, 1093–1095 (1993)
13. De Buck, S.S., Mackie, C.E.: Physiologically based approaches towards the prediction of pharmacokinetics: in vitro-in vivo extrapolation. *Expert Opin. Drug. Metab. Toxicol.* **3**, 865–878 (2007)
14. Falcone, A., Ricci, S., Brunetti, I., Pfanner, E., Allegrini, G., et al.: Phase III trial of infusional fluorouracil, leucovorin, oxaliplatin, and irinotecan (FOLFOXIRI) compared with infusional fluorouracil, leucovorin, and irinotecan (FOLFIRI) as first-line treatment for metastatic colorectal cancer: the Gruppo Oncologico Nord Ovest. *J. Clin. Oncol.* **1**;25, 1670–1676 (2007)
15. Filipski, E., Lemaigre, G., Liu, X.H., Mery-Mignard, D., Mahjoubi, M., Levi, F.: Circadian rhythm of irinotecan tolerability in mice. *Chronobiol. Int.* **21**, 613–630 (2004)
16. Garufi, C., Vanni, B., Aschelter, A.M., Zappala, A.R., Bria, E., Nisticó, C., Sperduti, I., Cognetti, F., Terzoli, E.: Randomised phase II study of standard versus chronomodulated CPT11 plus chronomodulated 5-fluorouracil and folinic acid in advanced colorectal cancer patients. *Eur. J. Cancer.* **42**, 608–616 (2006)
17. Gholam, D., Giacchetti, S., Brezault-Bonnet, C., Bouchahda, M., Hauteville, D., Adam, R., Ducot, B., Ghémard, O., Kustlinger, F., Jasmin, C., Lévi, F.: Chronomodulated irinotecan, oxaliplatin, and leucovorin-modulated 5-Fluorouracil as ambulatory salvage therapy in patients with irinotecan- and oxaliplatin-resistant metastatic colorectal cancer. *Oncologist.* **11**, 1072–1080 (2006)
18. Giacchetti, S., Itzhaki, M., Gruia, G., Adam, R., Zidani, R., Kunstlinger, F., Brienza, S., Alafaci, E., Bertheault-Cvitkovic, F., Jasmin, C., Reynes, M., Bismuth, H., Misset, J.L., Levi, F.: Longterm survival of patients with unresectable colorectal cancer liver metastases following infusional chemotherapy with 5-fluorouracil, leucovorin, oxaliplatin and surgery. *Ann. Oncol.* **6**, 663–669 (1999)
19. Granda, T.G., D'Attino, R.M., Filipski, E., Vrinaud, P., Garufi, C., Terzoli, E., Bissery, M.C., Levi, F.: Circadian optimisation of irinotecan and oxaliplatin efficacy in mice with Glasgow osteosarcoma. *Br. J. Cancer* **86**, 999–1005 (2002)
20. Guo, Y., Lu, P., Farrell, E., Zhang, X., Weller, P.: In silico and in vitro pharmacogenetic analysis in mice. *Proc. Natl. Acad. Sci. USA* **104**, 17735–17740 (2007)
21. Hansen, N.: The CMA evolution strategy: a comparing review. In: *Towards a new evolutionary computation. Advances on estimation of distribution algorithms*, pp. 75–102. Springer, Heidelberg (2006)
22. Izumo, M., Sato, T.R., Straume, M., Johnson, C.H.: Quantitative analyses of circadian gene expression in mammalian cell cultures. *PLoS Comput. Biol.* **2**, e136 (2006)
23. Kanno, Y., Otsuka, S., Hiromasa, T., Nakahama, T., Inouye, Y.: Diurnal difference in CAR mRNA expression. *Nucl. Recept.* **2**, 6 (2004)
24. Kormmann, B., Preitner, N., Rifat, D., Fleury-Olela, F., Schibler, U.: Analysis of circadian liver gene expression by ADDER, a highly sensitive method for the display of differentially expressed mRNAs. *Nucleic Acids Res.* **29**, E51–1 (2001)
25. Kuramoto, Y., Hata, K., Koyanagi, S., Ohdo, S., Shimen, H., Soeda, S.: Circadian regulation of mouse topoisomerase I gene expression by glucocorticoid hormones. *Biochem. Pharmacol.* **71**, 1155–1161 (2006)
26. Lavery, D.J., Lopez-Molina, L., Margueron, R., Fleury-Olela, F., Conquet, F.: Circadian expression of the steroid 15 alpha-hydroxylase (Cyp2a4) and coumarin 7-hydroxylase (Cyp2a5) genes in mouse liver is regulated by the PAR leucine zipper transcription factor DBP. *Mol. Cell. Biol.* **19**, 6488–6499 (1999)
27. Levi, F., Giacchetti, S., Zidani, R., Brezault-Bonnet, C., Tigaud, J., Goldwasser, F., Misset, J.L.: Chronotherapy of colorectal cancer metastases. *Hepatogastroenterology.* **38**, 320–322 (2001)

28. Levi, F., Okyar, A., Dulong, S., Innominato, P.F., Clairambault, J.: Circadian timing in cancer treatments. *Annu. Rev. Pharmacol. Toxicol.* **50**, 377–421 (2010)
29. Levi, F., Schibler, U.: Circadian rhythms: mechanism and therapeutics implications. *Annu. Rev. Pharmacol. Toxicol.* **47**, 593–628 (2007)
30. Morgan, D.: *The Cell Cycle, Principles of Control*. In: *Primers in Biology*. New Science Press Ltd and Oxford University Press, Oxford (2007)
31. Ohdo, S., Makinosumi, T., Ishizaki, T., Yukawa, E., Higuchi, S., Nakano, S., Ogawa, N.: Cell cycle-dependent chronotoxicity of irinotecan hydrochloride in mice. *J. Pharmacol. Exp. Ther.* **283**, 1383–1388 (1997)
32. Okyar, A., Piccolo, E., Ahowesso, C., Filipski, E., Hossard, V., Guettier, C., La Sorda, R., Tinari, N., Iacobelli, S., Levi, F.: Strain- and sex-dependent circadian changes in *abcc2* transporter expression: implications for irinotecan chronotolerance in mouse ileum. *PLoS One* **6**, e20393 (2011)
33. Ortiz-Tudela, E., Mteyrek, A., Ballesta, A., Innominato, P.F., Levi, F.: Cancer chronotherapeutics. Experimental, theoretical and clinical aspects. In: Kramer, A., Mellow, M. (eds) *Circadian clocks: overview and basic principles*, Springer, Heidelberg, in press
34. Panda, S., Antoch, M., Miller, B., Su, A., Schook, A.: Coordinated transcription of key pathways in the mouse by the circadian clock. *Cell* **109**, 307–320 (2002)
35. Pommier, Y.: Topoisomerase I inhibitors: camptothecins and beyond. *Nat. Rev. Cancer* **6**, 789–802 (2006)
36. Preitner, N., Damiola, F., Luis Lopez, M., Zakany, J., Duboule, D., Albrecht, U., Schibler, U.: The orphan nuclear receptor REV-ERB α controls circadian transcription within the positive limb of the mammalian circadian oscillator. *Cell* **110**, 251–260 (2002)
37. Slatter, J.G., Schaaf, L.J., Sams, J.P., Feenstra, K.L., Johnson, M.G., Bombardt, P.A.: Pharmacokinetics, metabolism, and excretion of irinotecan (CPT-11) following I.V. infusion of [(14)C]CPT-11 in cancer patients. *Drug. Metab. Dispos.* **28**, 423–433 (2000)
38. Smith, M.R., Burgess, H.J., Fogg, L.F., Eastman, C.I.: Racial differences in the human endogenous circadian period. *PLoS One* **4**, e6014 (2009)
39. Sothorn, R., Halberg, F., Hrushesky, W.: Circadian stage not time of day characterizes doxorubicin susceptibility rhythm of mice in continuous light. *Annu. Rev. Chronopharmacol.* **5**, 385–388 (1988)
40. Stanton, B.A.: Summary of the speaker presentations: ABC transporters in liver, kidney, and intestine. *Kidney International*, **62**, 1520–1521 (2002)
41. Storch, K.F., Lipan, O., Leykin, I., Viswanathan, N., Davis, F.C.: Extensive and divergent circadian gene expression in liver and heart. *Nature* **417**, 78–83 (2002)
42. Tsukamoto, Y., Kato, Y., Ura, M., Horii, I., Ishitsuka, H., Kusuhara, H., Sugiyama, Y.: A physiologically based pharmacokinetic analysis of capecitabine, a triple prodrug of 5-FU, in humans: the mechanism for tumor-selective accumulation of 5-FU. *Pharm. Res.* **18**, 1190–1202 (2001)
43. Welsh, D.K., Yoo, S.H., Liu, A.C., Takahashi, J.S., Kay, S.A.: Bioluminescence imaging of individual fibroblasts reveals persistent, independently phased circadian rhythms of clock gene expression. *Curr. Biol.* **14**, 2289–2295 (2004)
44. Zhang, Y., Yeager, R., Klaassen, C.: Circadian expression profiles of drug processing genes and transcription factors in mouse liver. *Drug Metab. Dispos.* **37**, 106–115 (2009)